



Culture of patient-derived multicellular clusters in suspended hydrogel capsules for pre-clinical personalized drug screening

Haijiang Dong^{a,b,c,d,1}, Zequn Li^{a,b,c,d,1}, Suchen Bian^{a,b,c,d,1}, Guangyuan Song^e,
Wenfeng Song^{a,b,c,d}, Mingqi Zhang^{f,g}, Haiyang Xie^{a,b,c,d}, Shusen Zheng^{a,b,c,d}, Xuxu Yang^{f,g,***},
Tiefeng Li^{f,g,**}, Penghong Song^{a,b,c,d,*}

^a Division of Hepatobiliary and Pancreatic Surgery, Department of Surgery, The First Affiliated Hospital, Zhejiang University School of Medicine, Zhejiang Province, Hangzhou, 310003, China

^b NHC Key Laboratory of Combined Multi-organ Transplantation, Zhejiang Province, Hangzhou, 310003, China

^c Key Laboratory of the Diagnosis and Treatment of Organ Transplantation, Research Unit of Collaborative Diagnosis and Treatment For Hepatobiliary and Pancreatic Cancer, Chinese Academy of Medical Sciences (2019RU019), Zhejiang Province, Hangzhou, 310003, China

^d Key Laboratory of Organ Transplantation, Research Center for Diagnosis and Treatment of Hepatobiliary Diseases, Zhejiang Province, Hangzhou, 310003, China

^e Department of Hepatopancreatobiliary Surgery and Minimally Invasive Surgery, Zhejiang Provincial People's Hospital (People's Hospital of Hangzhou Medical College), Zhejiang Province, Hangzhou, 310014, China

^f Center for X-Mechanics, Department of Engineering Mechanics, Zhejiang University, Zhejiang Province, Hangzhou, 310007, China

^g Key Laboratory of Soft Machines and Smart Devices of Zhejiang Province, Zhejiang Province, Hangzhou, 310007, China

ARTICLE INFO

Keywords:

Multicellular clusters
Hydrogel capsules
Tumor microenvironment
Tumor heterogeneity
Patient-derived tumor organoids
Personalized pre-clinical drug screening

ABSTRACT

A personalized medication regimen provides precise treatment for an individual and can be guided by pre-clinical drug screening. The economical and high-efficiency simulation of the liver tumor microenvironment (TME) in a drug-screening model has high value yet challenging to accomplish. Herein, we propose a simulation of the liver TME with suspended alginate-gelatin hydrogel capsules encapsulating patient-derived liver tumor multicellular clusters, and the culture of patient-derived tumor organoids (PDTOs) for personalized pre-clinical drug screening. The hydrogel capsule offers a 3D matrix environment with mechanical and biological properties similar to those of the liver *in vivo*. As a result, 18 of the 28 patient-derived multicellular clusters were successfully cultured as PDTOs. These PDTOs, along with hepatocyte growth factor (HGF) of non-cellular components, preserve stromal cells, including cancer-associated fibroblasts (CAFs) and vascular endothelial cells (VECs). They also maintain stable expression of molecular markers and tumor heterogeneity similar to those of the original liver tumors. Drugs, including cabazitaxel, oxaliplatin, and sorafenib, were tested in PDTOs. The sensitivity of PDTOs to these drugs differs between individuals. The sensitivity of one PDTO to oxaliplatin was validated using magnetic resonance imaging (MRI) and biochemical tests after oxaliplatin clinical treatment of the corresponding patient. Therefore, this approach is promising for economical, accurate, and high-throughput drug screening for personalized treatment.

1. Introduction

Chemotherapy and targeted drug therapy play critical roles in the treatment of liver tumors. However, owing to individual differences, the

traditional selection basis of clinical medication regimens fails to provide precise treatment for all patients [1]. Thus, a personalized medication regimen guided by pre-clinical drug screening is required for individualized precision treatment [2,3]. Specifically, pre-clinical drug

Peer review under responsibility of KeAi Communications Co., Ltd.

* Corresponding author. Division of Hepatobiliary and Pancreatic Surgery, Department of Surgery, The First Affiliated Hospital, Zhejiang University School of Medicine, Zhejiang Province, Hangzhou, China.

** Corresponding author. Center for X-Mechanics, Department of Engineering Mechanics, Zhejiang University, Zhejiang Province, Hangzhou, 310007, China.

*** Corresponding author. Center for X-Mechanics, Department of Engineering Mechanics, Zhejiang University, Zhejiang Province, Hangzhou, 310007, China.

E-mail addresses: xyyang@zju.edu.cn (X. Yang), litiefeng@zju.edu.cn (T. Li), songpenghong@zju.edu.cn (P. Song).

¹ These authors contributed equally to this work.

<https://doi.org/10.1016/j.bioactmat.2022.03.020>

Received 21 November 2021; Received in revised form 10 March 2022; Accepted 13 March 2022

Available online 19 March 2022

2452-199X/© 2022 The Authors. Publishing services by Elsevier B.V. on behalf of KeAi Communications Co. Ltd. This is an open access article under the CC BY-NC-ND license (<http://creativecommons.org/licenses/by-nc-nd/4.0/>).

screening models can be used to test the sensitivity of liver tumors to different drugs. In the process of drug screening, efficiency, economy, controllability, and operability are crucial criteria [4,5].

Drug screening liver tumor models developed to date include adherent liver cell lines, 3D culture liver cell lines, liver cell line-derived xenografts (CDXs), patient-derived xenografts (PDXs), and patient-derived organoids (PDOs) (Fig. 1A) [6]. However, these cell lines cannot effectively simulate the state of the original tumors, owing to changes in histological and genetic characteristics [7]. In the CDX and PDX models, tumor cell lines and patient-derived tumor tissues were implanted into immunodeficient mice. PDX simulates the original state of tumors better than cell lines; however, the difference in the origin of the species can lead to a certain difference in the therapeutic effect [8–10]. PDOs are organoids produced by culturing processed, patient-derived diseased tissue in a 3D matrix [11–13]; these are *in vitro* models established by stem cells or patient-derived primary cells based on a 3D *in vitro* cell culture system that can self-organize and resemble the corresponding organs or source tissues *in vivo* [14,15]. For example, patient-derived tumor cells can be cultured in hydrogels and commercialized Matrigel as patient-derived tumor organoids (PDTOs). The 3D matrix maintains spatial growth characteristics, which are similar to those of the extracellular matrix (ECM) *in vivo* [16–18]. The culture of PDTOs avoids the limitations of tumor size, degree of malignancy, and ethical animal problems [19,20].

Existing PDTOs derived from primary liver tumor single cells and co-cultures with immune cells cannot completely recapitulate the tumor microenvironment (TME), such as the biomechanical characteristics of ECM; fibroblasts and vascular-related cells of stromal cells; immune cells; and non-cellular components [21–24]. Numerous studies have reported that the TME can significantly influence tumor progression [25, 26]. For example, the biomechanical characteristics of organs affect the growth, invasion, and metastasis of tumor cells [27]. Cancer-associated fibroblasts (CAFs) promote tumor cell growth [28,29]. Vascularization maintains long-term survival and function of tumor cells [30,31]. The hepatocyte growth factor (HGF) mediates the interaction between tumor

and stromal cells, thereby promoting the movement, invasion, and metastasis of tumor cells [32,33]. Further investigations have also proven the connections between the mechanisms of action of drugs and stromal cells [34].

In this study, we simulated TME in PDTOs by culturing patient-derived multicellular clusters in hydrogels. Hydrogels composed of alginate and gelatin are produced as suspended capsules in the culture medium, which have similar mechanical and biological properties to tissues *in vivo*. As a result, we successfully cultured 18 PDTOs from 28 patient-derived liver multicellular clusters, with a success rate of 64.3%. Molecular markers of CAFs, vascular endothelial cells (VECs), and HGF were detected within the PDTOs, thereby validating the preservation of the liver TME. PDTOs also maintain stable expression of molecular markers and tumor heterogeneity, including genetic changes and tumor mutation burden (TMB). Thus, we performed personalized pre-clinical drug screening for liver tumors. We quantified the fluorescence microscopy images of live/dead cells stained after treating the PDTOs with cabazitaxel, oxaliplatin, or sorafenib. The sensitivity of the PDTOs showed individual differences between the drugs and their concentrations. The sensitivity of one PDTO to oxaliplatin was validated using magnetic resonance imaging (MRI) and biochemical tests after oxaliplatin clinical treatment of the corresponding patient. Our aim was to construct a new personalized pre-clinical drug screening model that expands the scope of drug applications and increases the accuracy, economy, and efficiency of clinical medications.

2. Results

2.1. Characteristics of alginate-gelatin hydrogel

We fabricated suspended hydrogel capsules to culture patient-derived multicellular clusters (Fig. 1B). The hydrogel networks were formed in 3D configurations with no restrictions on the growth of multicellular clusters. The mechanical properties of the hydrogel can be adjusted to iterate those of living tissues to better simulate the

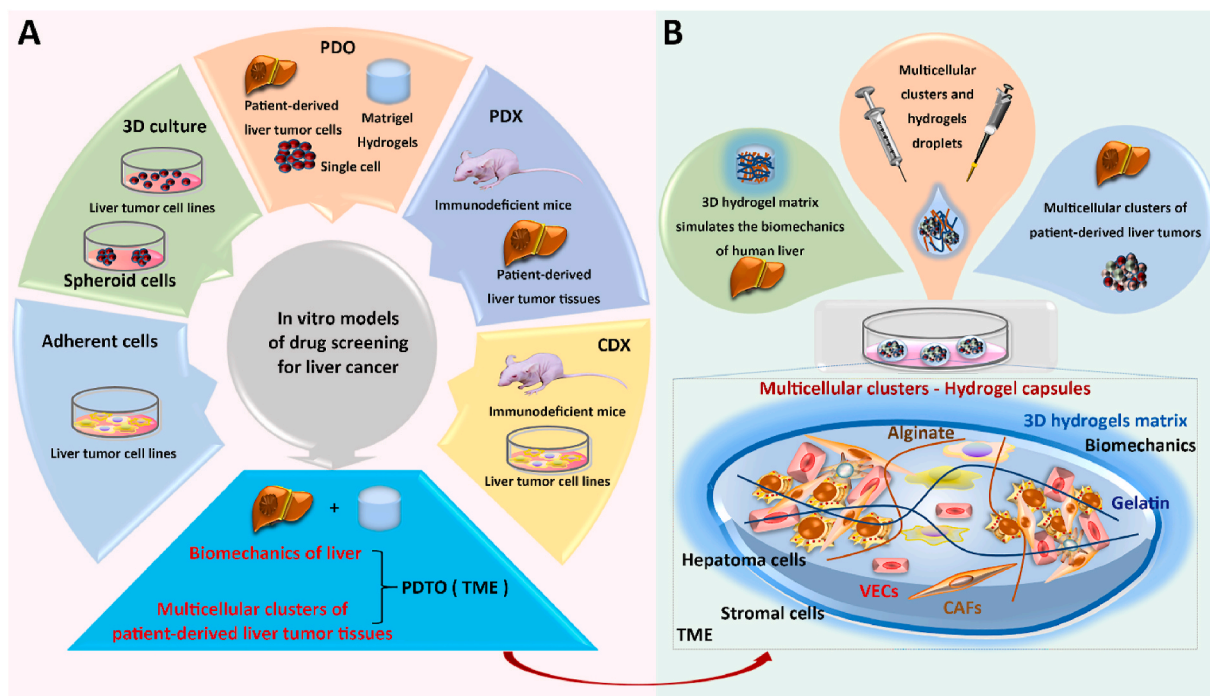


Fig. 1. Schematics of drug screening liver tumor models. A) Existing drug screening liver tumor models, including adherent liver cell lines, 3D culture liver cell lines, CDX, PDX, and PDO. PDTO is a kind of PDO, which can be derived from liver tumor multicellular clusters and possesses similar biomechanical characteristics as liver tissues. B) A 3D hydrogel matrix is produced with alginate and gelatin in a capsule form, which cultures liver tumor multicellular clusters containing hepatoma cells and stromal cells (CAFs and VECs) with preserved TME.

biomechanics of the ECM. Hydrogels in the form of suspended capsules efficiently exchange nutrients with the surrounding medium to support the metabolism of multicellular clusters. The cultured multicellular clusters were composed of hepatoma cells, stromal cells, and non-cellular components. As a result, the TME of multicellular clusters, similar to that of the original tumors, was preserved in the resultant PDTOs.

The mechanical properties of the hydrogels were adjusted by changing the proportion and crosslinking density of the networks. The hydrogels were comprised of crosslinked alginate and interpenetrated gelatin networks. We mixed gelatin with concentrations of sodium alginate varying from 0.5% (w/v) to 2% (w/v) and crosslinked its network with 75 mM or 100 mM CaCl_2 solution. Cells or multicellular clusters were planted in the hydrogels before crosslinking (Fig. 2A). After the hydrogels were cured, we first tested the modulus of the hydrogel without planting cells (Fig. 2B). The hydrogels with 0.5% (w/v) alginate, 0.25% (w/v) gelatin, and 75 mM CaCl_2 had a modulus of ~ 7.925 kPa, replicative of the human liver (7.0–7.5 kPa) [35]. Considering that the liver of most patients with liver cancer is fibrotic with a modulus above 7.5 kPa, we selected hydrogels with 75 mM CaCl_2 , 0.5% (w/v) alginate, and 0.25% (w/v) gelatin for the remaining

experiments.

We cultured HCCLM3 and HepG2 cells in hydrogels and tested their viability as a function of time. The cell counting Kit-8 (CCK-8) assay results showed that both HCCLM3 and HepG2 cells were in a state of continuous proliferation; there was no significant difference compared with the control group (Fig. 2C). The hydrogel did not restrict cell growth (Fig. 2D). The proliferation and division of cells were validated by optical and fluorescence observations as well as by fluorometric analysis (Fig. 2E, F, 2G).

We further verified the stability and degradability of the hydrogel capsules. The results showed that they maintained the consistency and integrity of their morphology within 15 days. On day 15, their weights in the control, HCCLM3, and PDT0 groups were 88.49%, 85.91%, and 87.85% of their initial weights, respectively (Fig. S1B). Meanwhile, PDT0 cultured to day 15 still maintained its multicellular morphology with good growth activity (Fig. S1C), while HCCLM3 cells maintained their morphology, activity, and division status (Fig. S1D). These results indicate that the physicochemical characteristics of the hydrogel capsules could meet the requirements for drug screening.

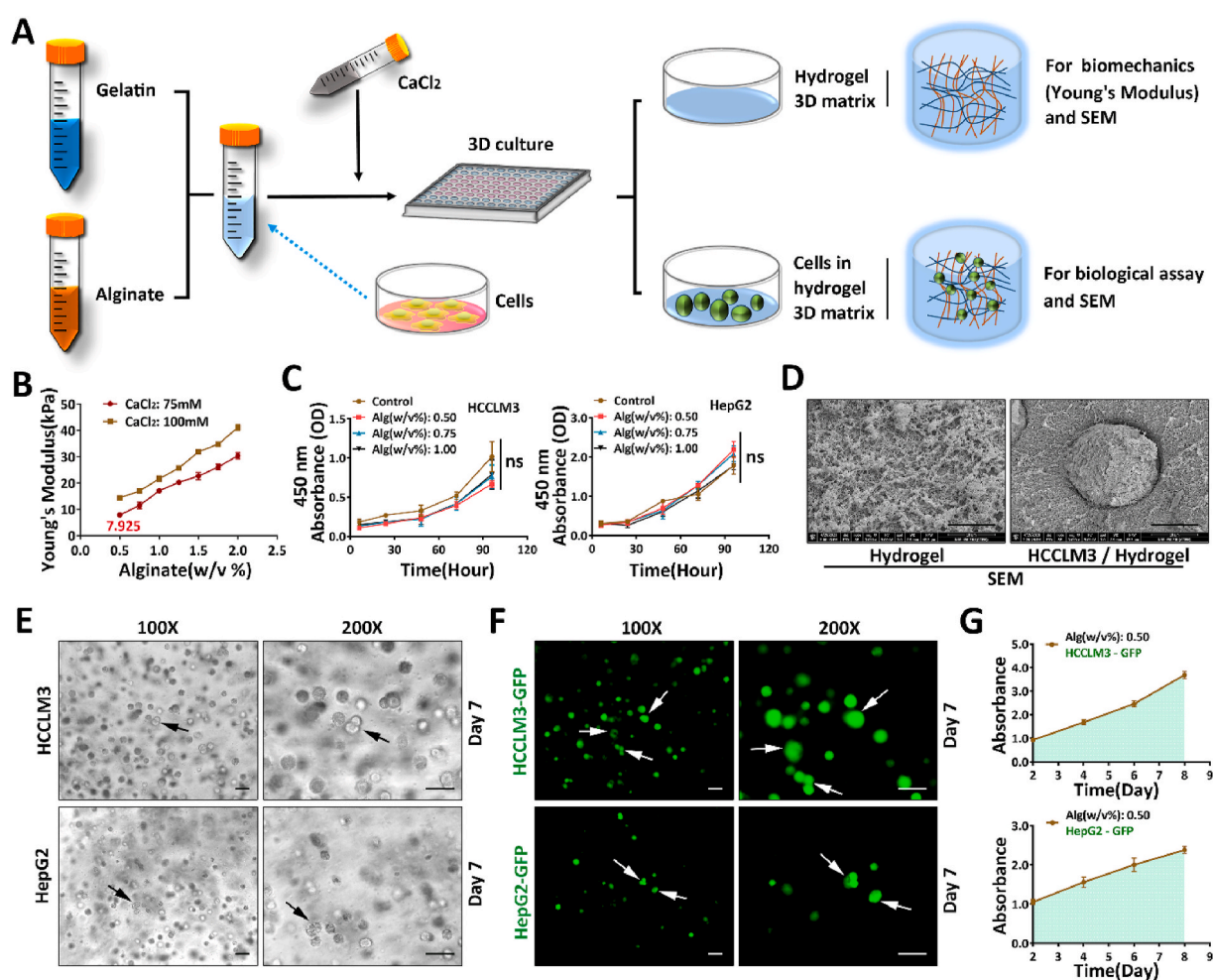


Fig. 2. Synthesis and characterization of the alginate-gelatin hydrogels. A) Schematic diagram of hydrogel preparation and cell culture. B) Young's modulus of hydrogel as a function of alginate concentration when the concentrations of gelatin and CaCl_2 were fixed at 0.25% (w/v) and at 75 mM or 100 mM, respectively. With 0.5% (w/v) alginate, 0.25% (w/v) gelatin, and 75 mM CaCl_2 , the hydrogel had a modulus of ~ 7.925 kPa, which was replicative of the human liver (7.0–7.5 kPa). C) HCCLM3 and HepG2 cells persistently proliferated in hydrogels; the cell viabilities showed no difference compared to the control groups. D) SEM images of hydrogel with and without HCCLM3 cells. Scale bar = 10 μm . E-F) Optical microscope (E) and fluorescence microscope (F) images of HCCLM3-GFP and HepG2-GFP cells cultured in hydrogel. The cells proliferate and divide during culture. The 100 X and 200 X represent the microscope magnification. Scale bar = 50 μm . G) Fluorometric assay results showing that HCCLM3-GFP and HepG2-GFP cells were in a state of continuous proliferation. All data shown are mean \pm SD; each data point represents 3–5 testing results.

2.2. PDO culture

We cultured PDOs in suspended hydrogel capsules, Matrigel, and hydrogel bulk for comparison (Fig. 3A). Matrigel is an extractive from Engelbreth-Holm-Swarm (EHS) murine sarcoma, has excellent biocompatibility, and has been widely used in 3D cellular and organoid cultures, such as liver tumor and pancreatic cancer organoids [36–38]. We digested patient-derived liver tumor tissues into single cells and multicellular clusters and suspended them in Matrigel or hydrogel precursors. Hydrogel capsules were prepared by dropping 10 μ L mixture of hydrogel precursor and suspension in 75 mM CaCl_2 solutions. We removed the residual CaCl_2 solution after the hydrogel was cured. The resultant capsules were suspended in the culture medium. After cultivation for 1–3 days, the planted cells and clusters started to proliferate and divide. We observed the morphology of the cells or clusters under a microscope and determined their viability (Fig. 3B). The successfully cultured living

clusters were PDOs, which preserved the characteristics of the original tumor tissues. We refer to the multicellular structures obtained by digestion before culture as clusters. After 5–7 days of culture in the 3D matrix, 3D structures similar to the corresponding source tissues were gradually formed through the self-organization of cells; these 3D structures are called organoids. We also cultured the Patient 28 derived single cells and multicellular clusters for 7 days. The live/dead cell staining results showed that the multicellular clusters and single cells had similar growth activity. However, the former featured an obvious multicellular structure that may contain stromal cells and some non-cellular components (Fig. 3C and D).

Comparisons were also made between PDOs in Matrigel, hydrogel bulk, and suspended hydrogel capsules. PDOs derived from two patients were cultured and observed. The PDOs cultured in three substrates showed similar multicellular structures and growth activity in both the optical and fluorescence microscope images (Fig. 4A, B, 4C).

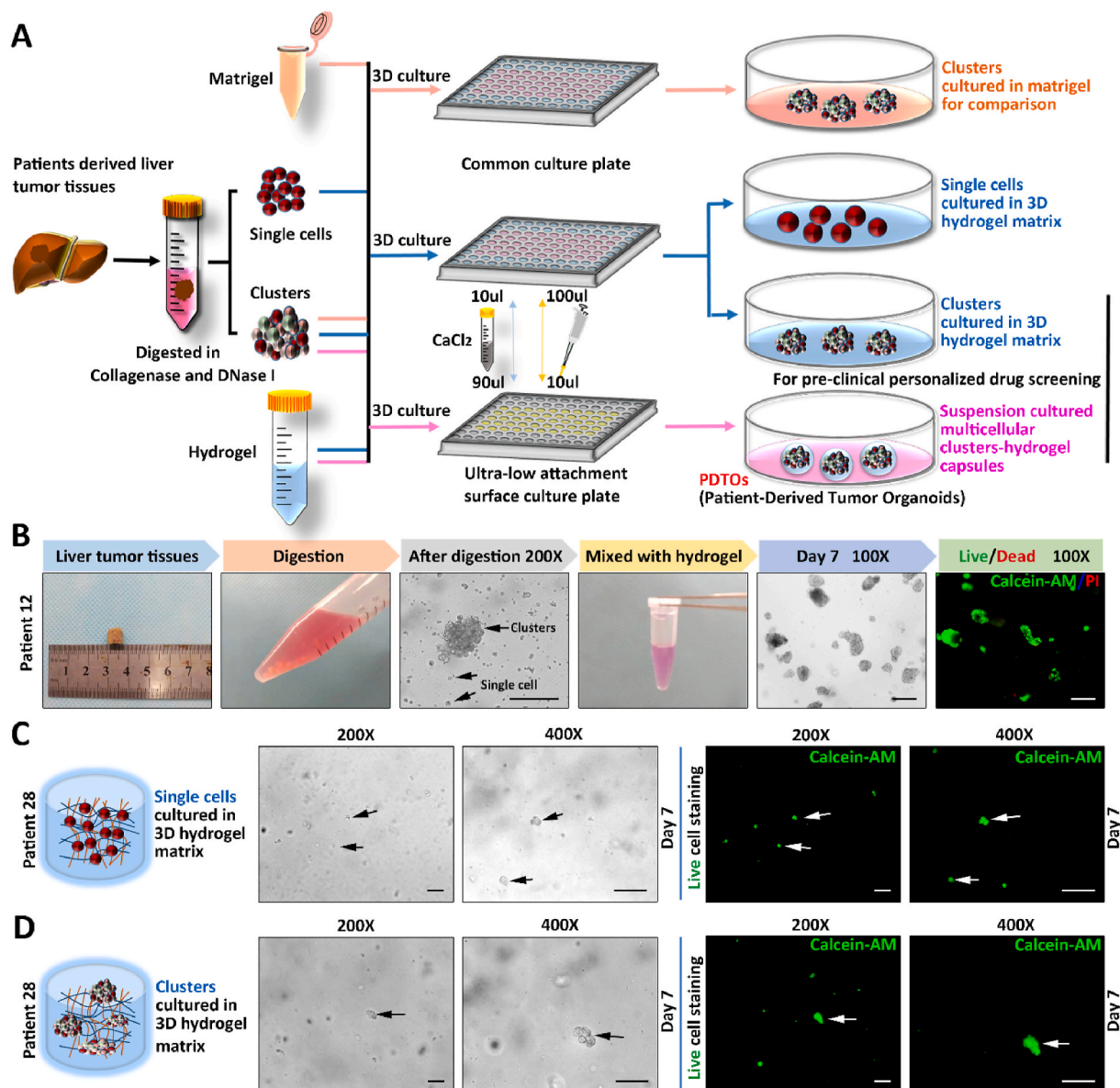


Fig. 3. Schematics and morphology outcome of PDO cultivation. A) PDO cultivation approaches, including multicellular clusters cultured in Matrigel (orange line), tumor single cells and multicellular clusters cultured in hydrogel bulks (blue line), and multicellular clusters cultured in hydrogel capsules (purple line). B) A patient-derived case shows the workflow of PDO cultivation and the activity detection of multicellular clusters. C) Optical microscope images of patient-derived liver tumor single cells cultured in hydrogel for 7 days as well as fluorescence microscope images of stained live cells. D) Optical microscope images of patient-derived liver tumor multicellular clusters cultured in hydrogel for 7 days as well as fluorescence microscope images of stained live cells. Scale bar = 100 μ m.

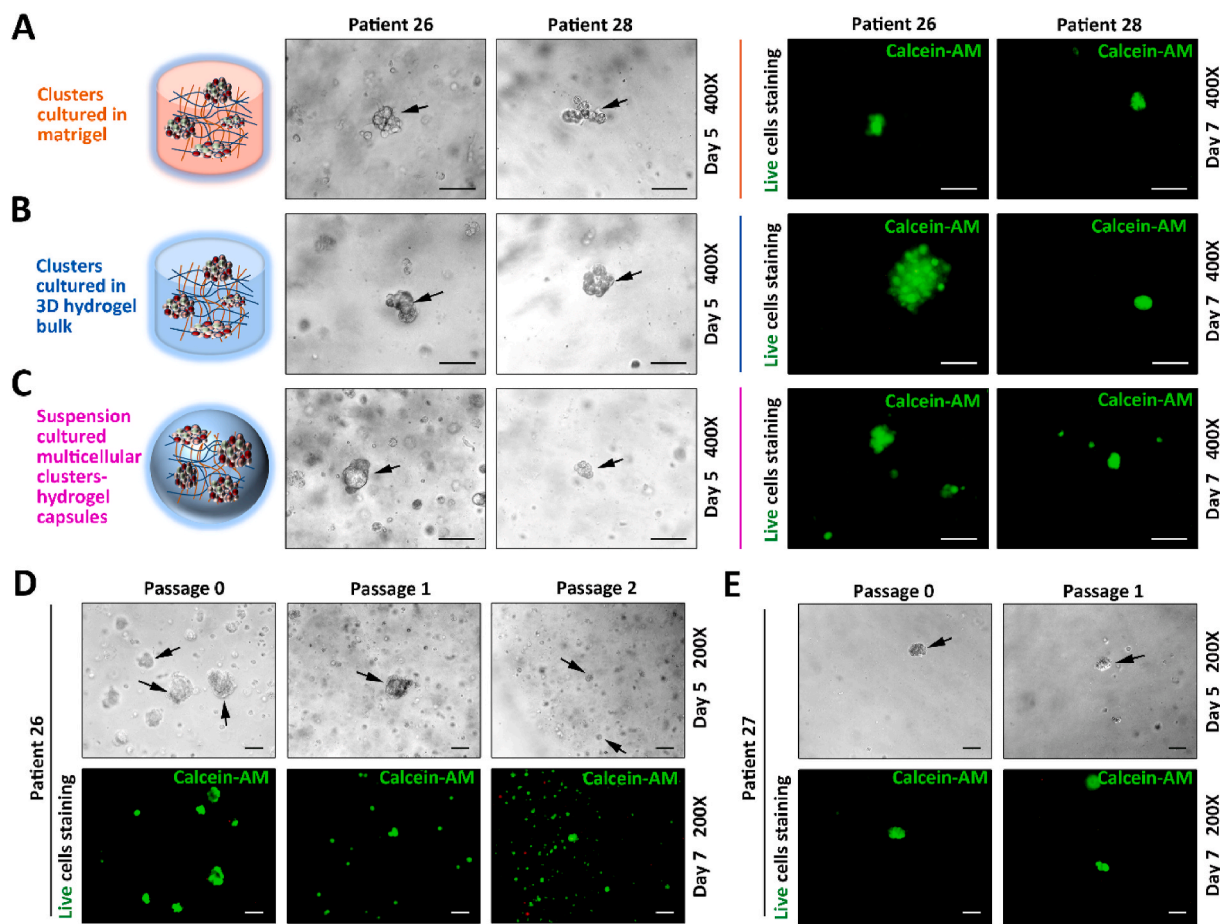


Fig. 4. Performance of cultured, passaged, cryopreserved, and recovered PDTOs. A-C) Multicellular clusters derived from Patients 26 and 28 were cultured in Matrigel, hydrogel bulk, and suspended hydrogel capsules for 5 days. They all presented multicellular structures under optical microscope. After culture for 7 days, stained live cells presented similar growth activity under fluorescence microscope for all cases. D) The multicellular clusters derived from Patient 26 in suspended hydrogel capsules maintained stable multicellular structures and growth activity during passage. E) Liver tumor tissues derived from Patient 27 were cryopreserved and recovered before culture in suspended hydrogel capsules. The resultant PDTOs still possessed stable multicellular structures and sufficient growth activity. Scale bar = 100 μm .

We also assessed the passage of PDTOs before and after cryopreservation and recovery. We dissociated the cultured PDTOs with ethylenediaminetetraacetic acid (EDTA) and cultured them in suspended hydrogel capsules for passage. Live/dead cell staining showed that the PDTOs maintained multicellular structures with good growth activity after multiple passages. The PDTOs were cryopreserved at $-80\text{ }^{\circ}\text{C}$ for a period of time; the passage of the recovered PDTOs was then observed. The recovered and cultured PDTOs maintained their multicellular structure and exhibited good growth activity (Fig. 4D). We also cryopreserved the tumor tissues at $-80\text{ }^{\circ}\text{C}$ for a period of time and constructed PDTOs upon recovery. The resultant PDTOs could also be cultured and passaged with complete multicellular structures and adequate growth activity (Fig. 4E).

2.3. Influence of patient and tumor conditions

We cultured PDTOs with 28 patient-derived liver tumor tissues; 18 of which were cultured successfully at a rate of 64.3% (Fig. 5). Among all 28 patients, the basic conditions such as basic diseases (hepatitis B virus [HBV] and hepatitis C virus [HCV]), liver function grade (Child-Pugh), alpha-fetoprotein (AFP), Barcelona Clinic Liver Cancer (BCLC) grade, and cirrhosis were different, as listed in Tables 1 and S1. Clinicopathological information such as tumor differentiation degree, growth pattern, size, number, and malignancy degree were also different, as listed in Tables S2 and S3. Additionally, the degree of tumor

differentiation was related to the degree of malignancy; the lower the degree of differentiation, the higher the degree of malignancy. Among the successfully cultured 18 PDTOs, one was poorly differentiated, five were moderately poorly differentiated, 11 were moderately differentiated, and one was highly moderately differentiated. This approach of PDTO culture was not limited by the degree of malignancy of the original tumor.

Among the successfully cultured 18 PDTOs, 17 HCC-PDTOs were derived from patients with hepatocellular carcinoma (HCC) and one CCC-PDTO was derived from a patient with cholangiocarcinoma (CCC). We found that the HCC-PDTOs had compact, solid, multicellular structures, whereas CCC-PDTO exhibited a lumen structure arranged with multiple cells. The continuously cultured CCC-PDTO presented multicellular clusters on day 1 and an obvious multicellular arrangement of lumen structure on day 7 (Fig. 6A and B). Consequently, this PDTO culture approach was not limited by the histological type of the original tumor. Moreover, we noted that all failure cases had cirrhosis; all cases without cirrhosis were successfully cultured. This approach of PDTO culture may be related to cirrhosis (Fig. 6C), but not to tumor histological type, basic diseases (HBV and HCV), liver function (Child-Pugh) grade, BCLC grade, AFP, tumor differentiation, malignancy, size, number, and growth pattern (Table S4). Other influences of underlying factors on the success rate of this approach require further studies.

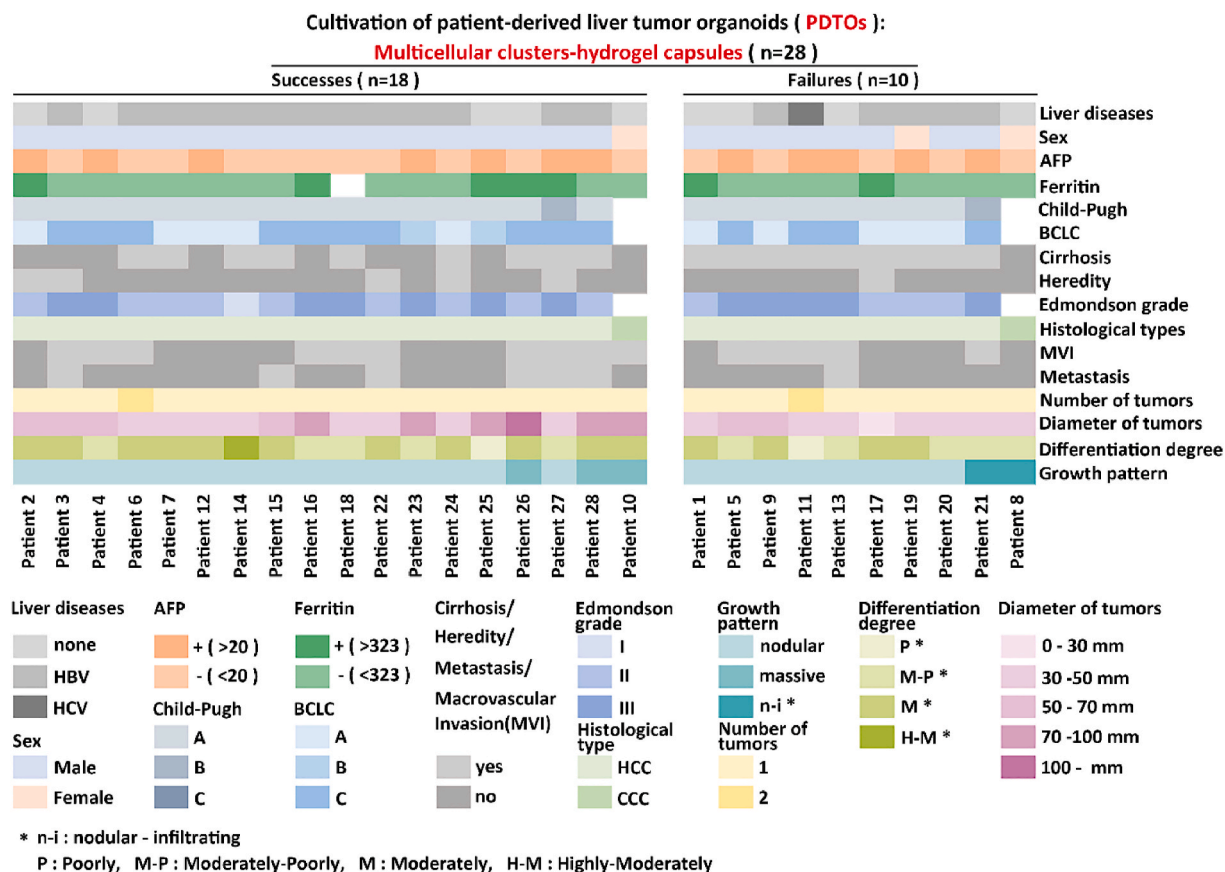


Fig. 5. A total of 18 PDTOs were successfully constructed by culturing 28 patient-derived multicellular clusters in suspended hydrogel capsules (success rate: 64.3%). The diversity of the successful cases showed that the constructions of PDTOs were not affected by variable factors, such as AFP, histological type of tumor, degree of tumor differentiation, malignant degree, HBV, HCV, liver function, tumor size, or growth pattern.

2.4. Preservation of TME and the stable expression of molecular markers

The cultured clusters contained not only hepatoma cells but also the TME, including stromal cells and non-cellular components. We detected the preserved TME in PDTOs using immunofluorescence staining of the molecular markers of the corresponding cells and components. The detected TME included stromal cell CAFs, VECs, and non-cellular components, such as HGF. Tubulin is a cytoskeletal component; the molecular markers of liver tumor cells include AFP, CK19, and glypican-3 (GPC-3); α -smooth muscle actin (α -SMA) and CD34 are molecular markers of CAFs and VECs, respectively. The confocal microscope images of immunofluorescence showed that tubulin was positively expressed; 3D imaging by confocal microscopy showed that multicellular clusters were arranged in 3D structures. Meanwhile, α -SMA and CD34 were positively expressed; 3D images indicated that the positive cells were arranged in a 3D structure, thereby indicating that the PDTOs contained 3D-distributed stromal cells, including CAFs and VECs (Fig. 6D, G, S2). Moreover, HGF was positively expressed and presented a 3D distribution, thereby indicating that the PDTOs contained non-cellular components (Fig. 6G, S2).

Hematoxylin-eosin (H&E) staining results showed that PDTOs maintained the morphology of the original tumor cells (Fig. 6E). Further immunofluorescence was performed on AFP, CK19, GPC-3, HGF, α -SMA, and CD34 in both PDTOs and original tumors. The expression of these molecular markers in PDTOs derived from both AFP (+) Patient 27 and AFP (-) Patient 26 was consistent with the original tumors and clinical pathological information (Fig. 6F and G, S2B). These results suggested that the PDTOs maintained stable expression of the molecular markers of the original tumors. In summary, PDTOs cultured with suspended hydrogel capsules preserved the main characteristics of the TME as well

as the stable expression of molecular markers of the original tumors.

2.5. Preservation of similar tumor heterogeneity to original tumors

Tumor heterogeneity affects growth rate, invasion ability, drug sensitivity, and prognosis [39,40]. Thus, we conducted whole-exome sequencing (WES) to compare the tumor heterogeneity of PDTOs, original tumors, and adjacent tissues. Tumor heterogeneity was reflected by genetic changes and TMB of WES results, where genetic changes were characterized by somatic copy number variation (CNV), single nucleotide variation (SNV), and mutation-related driver genes. CNV is caused by genome rearrangement, whereas SNV is caused by the substitution, insertion, or deletion of a single base. The mutation rate of the CNV locus is much higher than that of the SNV locus, which is an important pathogenic factor in human diseases [41]. TMB is the sum of somatic gene-coding errors, base substitutions, and gene insertions or deletions detected per million bases. It is a new marker for evaluating the therapeutic effect of immune checkpoint inhibitors and is related to the effect and prognosis of PD-1 and other immunotherapies [42].

The CNV results showed that the somatic total copy number, different allele copy number, minor allele copy number, as well as chromosome ploidy/purity of the PDTOs were identical to those of the original tumor from the same patient (Fig. 7A, S3). The PDTOs also expressed similar base substitutions to the original tumors, including C > T, C > A, C > G, T > C, T > A, T > G, as well as similar types of gene mutations to the original tumors, including Missense Mutation, Frame Shift Insert, Frame Shift Deletion, In Frame Insert, or In Frame Deletion. Moreover, TMB and mutation-related driver genes, including TP53, MUC17, and TTN, were also preserved in PDTOs. The consistency was validated in multiple patients; all PDTOs maintained similar tumor

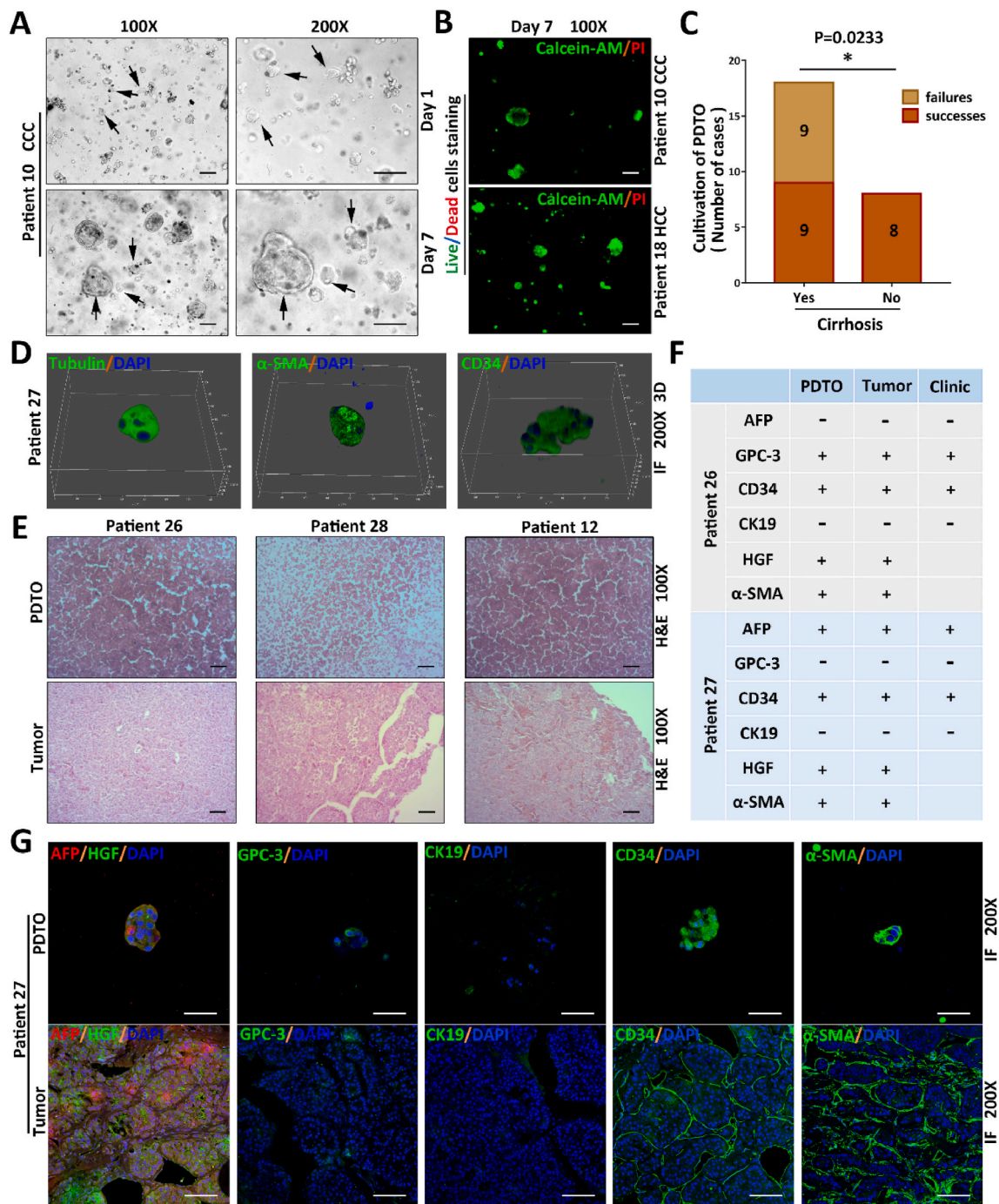


Fig. 6. PDTOs preserved the characteristics of TME and stable expression of molecular markers of the original tumors. A) Morphology of CCC-PDTOs on days 1 and 7, as captured by an optical microscope. The multicellular clusters proliferated and differentiated into lumen structures on day 7. B) Fluorescence microscope images of stained live/dead cells. The multicellular clusters in PDTOs maintained good activities and presented lumen or solid distribution on day 7. C) The comparative analysis of basic clinical and pathological information about 17 successful HCC-PDTOs and nine failed HCC-PDTOs. The success rate of PDTO cultivation was affected by cirrhosis. All data were shown as mean \pm SD and analyzed by two-sided Fisher's exact test. * $p < 0.05$. D) Immunofluorescence staining of PDTO derived from Patient 27; the 3D images of tubulin, α -SMA, and CD34 were captured under a confocal microscope. The PDTOs presented 3D distributed multicellular structures (tubulin [+]). Stromal cells, including CAFs and VECs in PDTOs, were preserved and presented a 3D distribution (α -SMA [+]) and CD34 [+]). E) Hematoxylin-Eosin (H&E) staining results of PDTOs and original tumors. F) The expressions of AFP, CD34, CK19, GPC-3, α -SMA, CD34, and HGF in PDTOs correspond with those in the original tumors and clinical pathological examination reports. G) Immunofluorescence staining of PDTO derived from Patient 27 and the original tumor. The expressions of AFP (+), CD34 (+), CK19 (-), GPC-3(-), α -SMA (+), and HGF (+) in PDTO correspond with those in the original tumor. Scale bar = 100 μ m.

heterogeneity to that of the original tumors (Fig. 7B).

2.6. Personalized drug screening

We tested the sensitivity of PDTOs to cabazitaxel (5 nM and 10 nM),

oxaliplatin (10 μ M and 20 μ M), and sorafenib (10 μ M and 20 μ M). Among them, cabazitaxel and oxaliplatin are commonly used in clinical tumor chemotherapy, while sorafenib is commonly used in targeted therapy [38,43,44]. After multicellular clusters were cultured to day 5–7 to form PDTOs, we started dosing and culturing the PDTOs for an

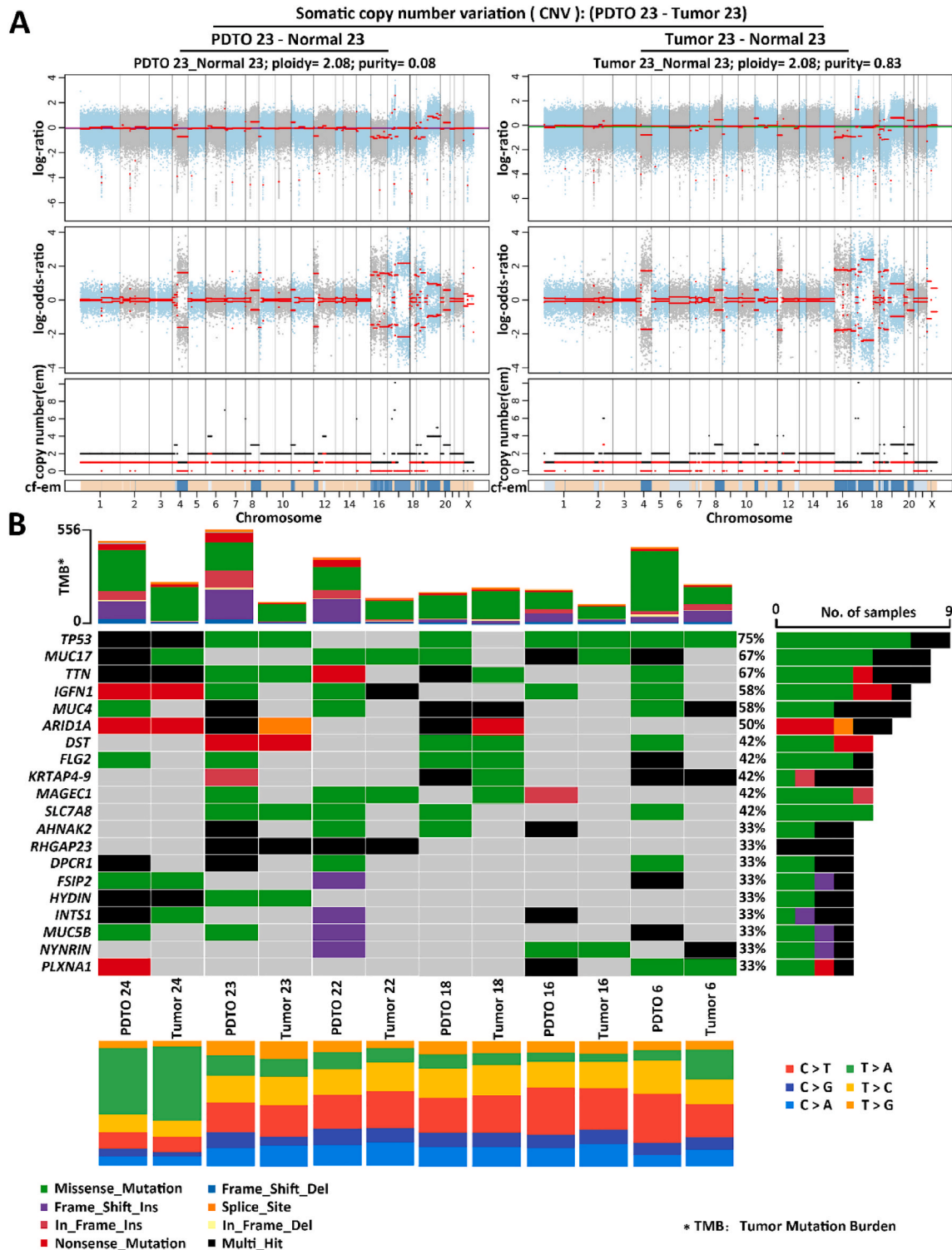


Fig. 7. The PDOs maintained the heterogeneity of original tumors. A) The PDO derived from Patient 23 presented similar somatic copy number variation to the original tumor, including total copy number, different allele copy numbers, minor allele copy numbers as well as chromosome ploidy. B) SNV, mutation-related driver genes, and TMB in the PDOs and original tumors were compared. The difference in base substitutions (C > T, C > A, C > G, T > C, T > A, and T > G), type of gene mutations (Missense Mutation, Frame Shift Insert, Frame Shift Deletion, In Frame Insert, and In Frame Deletion), mutation-related driver gene (TP53, MUC17, and TTN), and TMB between the PDOs and original tumors were small.

additional 7 days. Live/dead cell staining of the PDOs was imaged by confocal microscopy; the sensitivity of a PDO to a drug was quantitatively analyzed by comparing the dead/live cell ratio with and without dosing. The fluorescence/optical microscope images showed that the cells killed by the drugs presented aggregated fragment morphology

(Figs. 8A and S4). PDOs derived from multiple patients were tested. These patients exhibited histological types of CCC and HCC. Different sensitivities were observed for each individual (Fig. 8B and C, S5). We noted that PDOs from different patients reacted differently to different drugs at various concentrations. For example, PDOs derived from

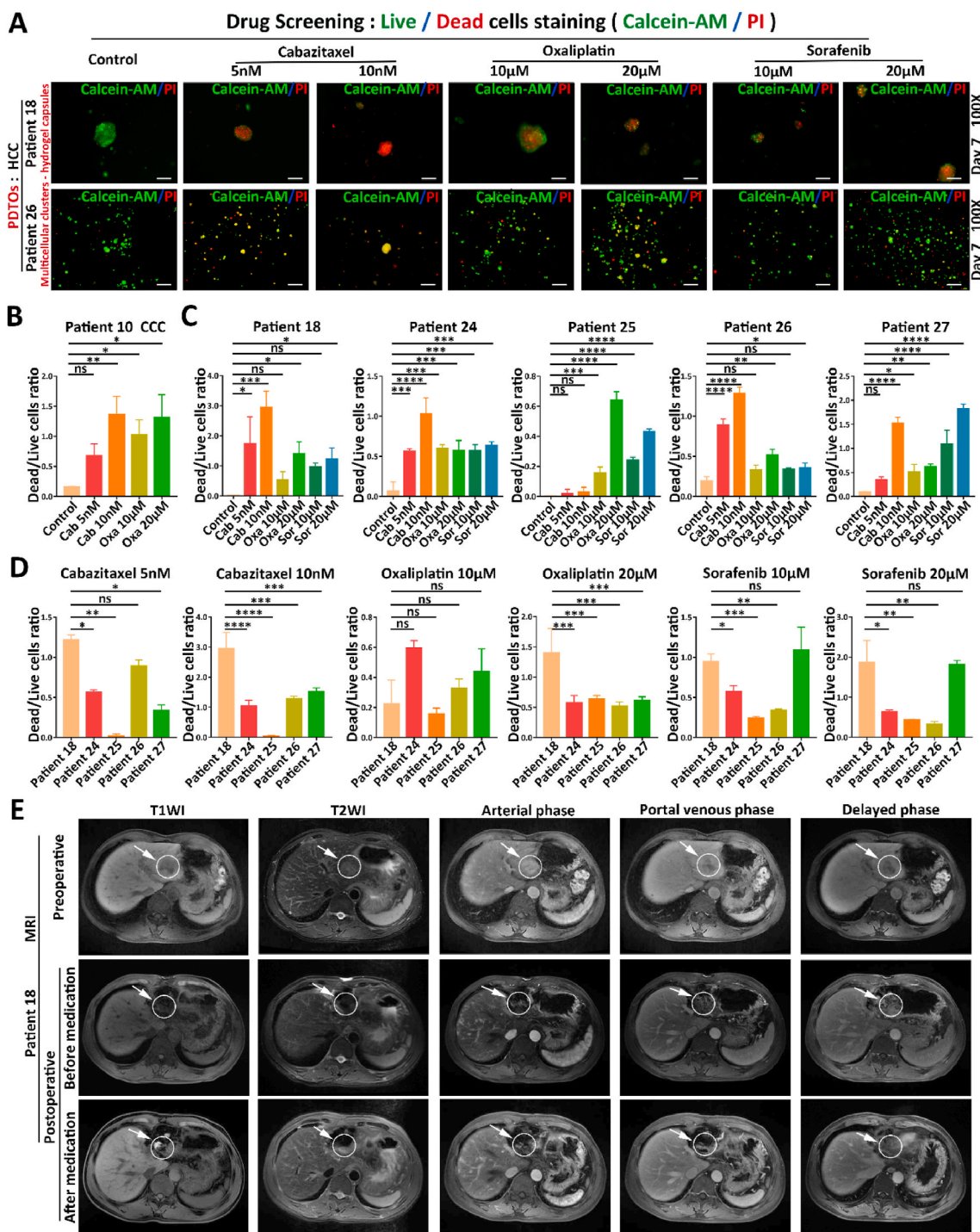


Fig. 8. Personalized drug screening by PDTOs. A) PDTOs derived from Patients 18 and 26 were cultured for 7 days with different drugs. Scale bar = 100 µm. B-D) The dead/living cell ratio of CCC-PDTo derived from Patient 10 in response to drugs with different concentrations. (B) The dead/living cell ratio of HCC-PDTo derived from Patients 18, 24, 25, 26, 27 in response to drugs with different concentrations. (C) In response to the same drug with identical concentration, the dead/living cell ratio of HCC-PDTo derived from different patients varied accordingly. (D) All data were shown as mean ± SD and analyzed by one-way ANOVA. *p < 0.05, **p < 0.005, ***p < 0.001, ****p < 0.0001, ns = not significant. E) Patient 18 was treated with oxaliplatin for 3 months after operation. Comparing the pre-operative and post-operative MRI results before and after medication, the T1WI, T2WI, arterial, portal venous, and delayed phases showed no blood flow signal or tumor recurrence. The circular area indicated by the arrow was the surgical area. The tested sensitivity of PDTOs derived from Patient 18 to oxaliplatin was validated by the MRI evaluation after clinical oxaliplatin treatment.

Patients 18 and 26 were the most sensitive to cabazitaxel, PDTOs derived from Patient 25 were the most sensitive to sorafenib and 20 mM oxaliplatin, and PDTOs derived from Patient 27 were the most sensitive to sorafenib. With only two concentrations tested, the death rate increased for cells in PDTOs from most patients when higher

concentrations of drugs were used. In response to the same drug at identical concentrations, HCC-PDTo from different patients also showed different sensitivities (Fig. 8D).

Furthermore, we followed the conditions of Patient 18, who was treated with oxaliplatin. The sensitivity of the PDTOs derived from this

patient to oxaliplatin was demonstrated in our study. Although the sensitivity to oxaliplatin was not as high as that to cabazitaxel, dead cells outnumbered live cells after administration of 20 μM oxaliplatin. We compared the results of MRI and biochemical tests before and after the administration of oxaliplatin for 3 months. The different phases of MRI, including T1WI, T2WI, arterial, portal venous, and delayed phases, showed no blood flow signal or tumor recurrence in the operation area (Fig. 8E). We also established from the biochemical test results that liver function was in a normal state after therapy. Total bile acid (TBA) and carcinoembryonic antigen (CEA) levels also returned to normal (Table S5). The sensitivity of Patient 18 liver tumors to oxaliplatin was validated by the results of the MRI and biochemical tests.

3. Discussion

In this study, suspended hydrogel capsules were used to culture PDTOs. Hydrogels were produced using alginate and gelatin networks. These two polymer networks, which originate from nature, are considered economical and with excellent biocompatibility for cultivation [45–48]. With the acquainted components of the hydrogel, the mechanical properties, network density, and grafted functional groups can be easily adjusted to better simulate the ECM [49]. The hydrogels were synthesized with PBS, while the material exchange between the hydrogel and external medium was continuous; thus, the metabolism of cells inside the hydrogels was well-supported. We used capsulated hydrogels suspended in a culture medium. The interface area of the hydrogel and medium was much larger than that of the bulk hydrogel with the same volume. The exchange of metabolic products and nutrition was faster in the hydrogel capsules. As a result, the success rate of cultivation was as high as 64.3%. The hydrogels used for culture were extremely cheap (about US\$0.005 per milliliter) compared to the commonly used Matrigel (approximately US\$ 60 per milliliter). Multiple drugs could be screened using our model for 10 days. In addition, there were alternative formation processes for hydrogels; PDTOs can also be produced with hydrogels through 3D bioprinting [50,51], microfluidics [52–54], or organ/tumor-on-a-chip [55–57]. The cycle of our method was short; high-throughput drug screening can be completed within 7–10 days. Consequently, our strategy was efficient and exhibited outstanding controllability and operability.

Our PDTOs were cultured from tissue clusters. As such, they simulated both the biomechanical and biological characteristics of TME. By changing the crosslinker density, we can modify the hydrogel modulus to mimic that of the diseased liver. Currently, we only used one modulus, since the relevant modulus of patient organs was not measured; thus, we synthesized hydrogels mimicking the modulus of a healthy liver. However, organ modulus can be measured by methods such as ultrasound [58–60]; we can adjust the hydrogel modulus and simulate each patient's organ conditions. Although only two types of stromal cell components (CAFs and VECs) and one type of non-cellular component (HGF) were tested, we believe that other factors influencing tumor cell growth were also preserved. The TME was preserved as closely as possible to the original tumor. As a result, the PDTOs expressed molecular markers identical to those of the original tumors. Thus, the tumor heterogeneity was minimally changed. Precisely simulating the TME greatly expands the range of applicable drugs for a more accurate screening. Moreover, this method was not limited by the histological type or degree of malignancy of the original tumor. We tested the sensitivities of our PDTOs to cabazitaxel, oxaliplatin, and sorafenib; however, other types of drugs and drug combinations can also be evaluated for screening to obtain a precise personalized medication regimen. In the future, more information on cellular organization in the model should be detected. In addition, we will further collect tumor samples, screen a variety of combination drugs through cultured PDTOs, and further compare the effects with clinical combination drugs.

In addition, higher fidelity of *in vitro* models has been achieved by vascularization [61,62], multicellular co-culture [63–65], tissue

engineering [66–68], tissue decellularization [69,70] and genetic technologies [71–73]. It is expected that more components of the TME will be introduced into PDTOs in the future by applying these methods [74–76]. Organoids cultured using some novel approaches can be further applied in basic physiological research, drug development, regenerative medicine, and organ replacement therapies [77–80] for a higher degree of personalized and precision therapy [81,82].

4. Conclusion

In summary, we encapsulated patient-derived liver tumor multicellular clusters in suspended hydrogel capsules and cultured PDTOs. These PDTOs preserved the characteristics of the TME, stable expression of molecular markers, and heterogeneity of the original liver tumors. Our method has several advantages, including easy operation, low cost, high success rate, high simulation degree, short cycle, and high throughput. Moreover, it is not limited by the histological type or degree of malignancy of the liver. The proposed approach is promising for the construction of a personalized drug-screening model that can increase the accuracy, economy, and efficiency of clinical medication and further promote the implementation of precision medicine.

5. Materials and methods

5.1. Preparation of alginate-gelatin hydrogel precursor

Gelatin (V900863, Sigma-Aldrich) at a concentration of 0.25% (w/v) and sodium alginate (A0682, Sigma-Aldrich) at concentrations of 0.5%, 0.75%, 1%, 1.25%, 1.5%, 1.75%, and 2% (w/v) were dissolved in PBS (pH = 7.4, BI) by stirring and heating at 70 °C in a water bath for 30 min. The solution was stored at 4 °C in a refrigerator until subsequent use.

5.2. Mechanical tests of hydrogels

The alginate-gelatin precursors were crosslinked into hydrogels by mixing them with CaCl_2 solutions. The precursors were poured into 24-well culture plates, whose bottoms were covered with CaCl_2 solutions (75 mM and 100 mM). The precursors were cured for 48 h and then soaked in PBS for another 48 h. The hydrogels were then loaded into a mechanical testing machine (100 N load cells; Instron Model 5966) using a compression fixture with a fixed loading rate of 0.5 mm/min.

5.3. Cell culture

For cell culture in the hydrogel, HCCLM3-GFP and HepG2-GFP cell suspensions were mixed with equal volumes of hydrogel precursors as a cell-hydrogel mixture. The bottom of a 96-well culture plate was filled with 10 μL of 75 mM CaCl_2 solution, followed by dripping 90 μL of the cell-hydrogel mixture into the wells. The culture plate was kept in an incubator at 37 °C for 30 min until the hydrogel was cured. Then, 150 μL of the culture medium was added to each well. The medium was changed every 2 days.

The control group used conventional cell culture medium, whereas the experimental group used the above-mentioned cell culture medium soaked with different concentrations of hydrogel. Then, they were cultured in the conditions of 37 °C and 5% CO_2 for 6, 24, 48, 72, and 96 h. The proliferation status and activity of cells were assayed using the Cell Counting Kit-8 (CCK-8, MCE) and Multimode Reader (Thermo Fisher).

5.4. Scanning electron microscopy

Cured hydrogels with and without cells were subjected to scanning electron microscope (SEM) observation. The samples were fixed in 1% glutaraldehyde (Sigma-Aldrich) for 1 h, rinsed in PBS, dehydrated in a graded series of ethanol (30%, 50%, 70%, 90%, 100%), dried via critical

point drying using a liquid CO₂ dryer (Tousimis 931 GL), and imaged using an SEM (Nova Nano 450, Thermo FEI) at 5.0 kV.

5.5. Patient-derived liver tumor specimens

Fresh liver tumor tissues were collected with informed consent from the surgical patients at the First Affiliated Hospital, School of Medicine, Zhejiang University (Hangzhou, China). This study of patient liver tumor specimen collection was approved by the Clinical Research Ethics Committee of the First Affiliated Hospital, College of Medicine, Zhejiang University (Project Number: 2020C04003). Fresh liver tumor tissue was obtained in the operating room, placed it into a sterile centrifugal tube pre-added with cold PBS, and then stored in an icebox, which was quickly transferred to the laboratory within 20 min for further operation. Related clinical information is available in Table 1 and Tables S1–S3 (Support Information).

5.6. Digestion and cryopreservation of patient-derived liver tumor tissues

Patient-derived tumor tissues were washed with PBS, cut into 2–3 mm pieces, and centrifuged at 600 rpm for 2 min. Subsequently, they were digested in a solution containing 2.5 mg/mL collagenase IV (Gibco) and 0.1 mg/mL DNase I (Sigma-Aldrich) for 5–8 min, followed by centrifugation at 600 rpm for 3 min and washing with PBS to obtain multicellular clusters. Single cells were obtained by digestion for 30 min. The excised fresh liver tumor tissues were cut into 3–5 mm pieces, washed with cold PBS, and cryopreserved in a cryopreservation solution containing fetal bovine serum (FBS, BI) and dimethyl sulfoxide (DMSO, Sigma-Aldrich) at a volume ratio of 9:1.

5.7. Cultivation, passage, cryopreservation and recovery of PDTOs

PDTOs were cultured in three forms: 1) Cultures of multicellular clusters in Matrigel were produced by mixing a suspension of multicellular clusters and Matrigel (Corning) in equal proportions as well as adding a culture medium after incubation at 37 °C for 30 min; 2) Cultures of multicellular clusters/single cells in alginate-gelatin hydrogel precursor were produced by mixing multicellular clusters/single cell suspension and alginate-gelatin hydrogel precursor in equal proportions, adding 75 mM CaCl₂ at a volume ratio of 10%, and curing in a 37 °C incubator for 20 min; 3) Cultures of multicellular clusters in suspended hydrogel capsules were produced by mixing a suspension of multicellular clusters and alginate-gelatin hydrogel precursor in equal proportions, dropping the mixture in ultra-low attachment surface 96-

well culture plates containing 75 mM CaCl₂, and adding the culture medium after removal of the CaCl₂ solution. The volume of each droplet was 10 µL. The PDTO culture medium consisted of the following agents: advanced DMEM/F-12 (Gibco) supplemented with B-27 (1:50; Gibco), N-2 (1:100, Gibco), HEPES (1:1000, Gibco), penicillin (1:100, Solarbio), nicotinamide (10 mM, Sigma-Aldrich), N-acetyl-L-cysteine (1.25 mM, Sigma-Aldrich), gastrin 1 (10 nM, MCE), forskolin (10 µM, MCE), EGF (50 ng/mL, PeproTech), FGF10 (100 ng/mL, PeproTech), HGF (25 ng/mL, PeproTech), R-spondin 1 (100 ng/mL, PeproTech), noggin (100 ng/mL, PeproTech), and Wnt3a (100 ng/mL, Fitzgerald). We dissociated the PDTOs from the hydrogel by adding 3.5 mM ethylenediaminetetraacetic acid (EDTA); the recovered PDTOs from cryopreservation could be passaged and cultured as before preservation.

5.8. Stability and degradability test of hydrogel capsules

According to those previously outlined, hydrogel capsules were prepared in 20 mm petri dishes for culturing HCCLM3 cells and liver tumor multicellular clusters (2 × 10⁵ cells/mL). The group without cells was used as the control. The hydrogel capsules were embedded in the culture medium to maintain swelling ratios. The aseptic states of the hydrogel were maintained by the following procedure: On days 1, 3, 6, 9, 12, and 15, the medium around the hydrogel capsules was removed. Subsequently, they were weighed and snapshotted immediately in a biological safety cabinet.

5.9. H&E and immunofluorescence staining

The original tumor tissues were stored in 10% formalin, paraffin-embedded, dehydrated, and sliced for staining. After the PDTOs were dissociated from the hydrogel, they were either smeared on glass slides for H&E staining or transferred to 20-mm glass bottom cell culture dishes (NEST) for immunofluorescence staining. The samples were then fixed with 4% paraformaldehyde for 30 min, washed three times with PBS, added with 100 µL 0.5% Triton X-100, and incubated at room temperature for 30 min. Subsequently, the samples were washed again three times with PBS and blocked with 5% bovine serum albumin (BSA)/PBS solution at 37 °C for 30 min. Next, anti-AFP (1:100, Abcam), anti-CD34 (1:200, Abcam), anti-HGF (1:50, Abcam), anti-CK19 (1:200, Abcam), anti-tubulin (1:200, Abcam), anti-GPC-3 (1:500, Abcam), and anti-α-SMA (1:200, Abcam) antibodies diluted in 0.1% BSA/PBS were added, followed by incubation overnight at 4 °C. Next, the samples were incubated with goat anti-rabbit/mouse secondary antibody (1:200, Thermo Fisher) in 0.1% BSA/PBS and preserved at 37 °C for 2 h after

Table 1
Clinical data of patients (Successes).

Patient	Sex	Age (Years)	Drinking History	Tumor	Liver Disease	Cirrhosis	Ferritin (ng/mL)	AFP (IU/mL)	Child Pugh	BCLC	Heredity
2	M	78	no	HCC	none	no	562.8	20.7	A	A	yes
3	M	45	yes	HCC	HBV	no	309.8	3.6	A	C	yes
4	M	71	yes	HCC	none	no	223	84.8	A	C	no
6	M	51	yes	HCC	HBV	yes	309.9	4	A	C	no
7	M	74	yes	HCC	HBV	yes	243.4	1.1	A	A	no
12	F	68	no	HCC	HBV	no	163	70.8	A	A	no
14	M	66	yes	HCC	HBV	yes	210.3	8.5	A	A	no
15	M	68	no	HCC	HBV	yes	282	2.1	A	C	no
16	M	67	no	HCC	HBV	no	467.1	3.9	A	C	no
18	M	53	no	HCC	HBV	yes	—	2.7	A	C	no
22	M	67	no	HCC	HBV	no	198.5	3.1	A	C	yes
23	M	58	no	HCC	HBV	no	228.2	909.8	A	B	no
24	M	63	no	HCC	HBV	yes	265.4	3.9	A	A	yes
25	M	75	no	HCC	none	no	435	22.9	A	B	no
26	M	59	no	HCC	none	yes	557.7	4.1	A	C	no
27	M	58	no	HCC	HBV	yes	613.7	111.7	B	C	yes
28	M	34	no	HCC	HBV	yes	62.6	4099.4	A	C	no
10	F	62	no	CCC	none	no	104.6	1.7	—	—	no

M: Male, F: Female, HCC: Hepatocellular Carcinoma, CCC: Cholangiocarcinoma. HBV: Hepatitis B Virus, AFP: Alpha-fetoprotein, BCLC: Barcelona Clinic Liver Cancer.

washing three times with PBS. Finally, DAPI was applied and the samples were incubated for another 10 min. Immunofluorescence imaging was performed on a Zeiss LSM 710 confocal microscope.

5.10. Whole exome sequencing

WES was performed on PDOs, original tumors, and adjacent tissues, and supported by Hangzhou LC-BIO Co., Ltd. DNA enrichment of all exons was performed using an Agilent SureSelectXT capture system (Agilent. Co.); high-throughput sequencing was conducted using a NovaSeq 6000 sequencer. Library construction and capture experiments were performed using the Agilent SureSelect Human All Exon V6 kit.

Prior to alignment, low-quality reads were removed using fastp. For alignment, Burrows Wheeler Aligner (BWA) was used to align reads to the reference genome (hg19). During the first post-alignment processing step, Picard tools were used to identify and mark duplicate reads from the BAM file. Base quality score recalibration was then performed prior to variant calling to reduce systematic biases. Somatic SNVs and InDels were jointly called Mutect2 and Strelka; only variants that passed both quality filters were included in the follow-up analysis. A variant effect predictor (VEP) was used to add biological information to the variant set. Copy number variations were detected using Control-FreeC. The GC content of the sequences was used to normalize the read distribution; the normalized distribution of aligned reads in slide windows was used to calculate the copy number difference between the tumor and normal samples.

5.11. Live/dead cell staining and drug screening

Live/dead cell staining was performed using a Calcein-AM/PI Double Staining Kit (Dojindo). The staining solution was prepared with PBS; the concentrations of Calcein-AM and PI were 2 μM and 4.5 μM , respectively. The samples were immediately imaged using an Olympus Fluoview FV1000 confocal microscope after incubation at 37 °C for 20 min.

For drug screening, the PDOs constructed by the above-mentioned methods were tested with cabazitaxel (5 nM and 10 nM, MCE), oxaliplatin (10 μM and 20 μM , MCE), and sorafenib (10 μM and 20 μM , MCE). Dosing was started after the PDOs were cultured for 5 days. Then, they were cultured for another 7 days. Live/dead cell staining of PDOs was imaged by confocal microscopy for quantitative analysis.

5.12. Statistical analysis

All data are shown as mean \pm SD. Statistical analysis was performed using two-sided Fisher's exact test and one-way ANOVA. Significance levels were determined as * $p < 0.05$, ** $p < 0.005$, *** $p < 0.001$, **** $p < 0.001$, and ns = not significant ($p > 0.05$).

CRediT authorship contribution statement

Haijiang Dong: Conceptualization, Methodology, Investigation, Data curation, Formal analysis, Visualization, Writing – original draft, Writing – review & editing. **Zejun Li:** Methodology, Investigation, Data curation, Formal analysis, Visualization, Writing – original draft, Writing – review & editing. **Suchen Bian:** Methodology, Investigation, Formal analysis, Visualization, Writing – original draft, Writing – review & editing. **Guangyuan Song:** Methodology, Formal analysis, Investigation. **Wenfeng Song:** Methodology, Visualization, Data curation. **Mingqi Zhang:** Formal analysis, Software, Visualization. **Haiyang Xie:** Methodology, Investigation, Resources. **Shusen Zheng:** Resources, Supervision. **Xuxu Yang:** Conceptualization, Methodology, Resources, Formal analysis, Supervision, Funding acquisition, Project administration, Writing – review & editing. **Tiefeng Li:** Conceptualization, Methodology, Resources, Formal analysis, Supervision, Funding acquisition, Project administration, Writing – review & editing. **Penghong Song:** Conceptualization, Methodology, Resources, Formal analysis,

Supervision, Funding acquisition, Project administration, Writing – review & editing.

Declaration of competing interest

The authors declare no conflict of interest.

Acknowledgements

This work was supported by the Key Research and Development Plan of Zhejiang Province (No. 2020C04003), the National Natural Science Foundation of China (No. 82070652, No. 81870434, NO. T2125009, NO. 92048302, NO. 11822207 and NO. 12102388), the Natural Science Foundation of Zhejiang Province (NO. LR18A020001) and the Research Project of Jinan Microecological Biomedicine Shandong Laboratory (JNL-2022007B).

Appendix A. Supplementary data

Supplementary data to this article can be found online at <https://doi.org/10.1016/j.bioactmat.2022.03.020>.

References

- [1] X. Xia, F. Li, J. He, R. Aji, D. Gao, Organoid technology in cancer precision medicine, *Cancer Lett* 457 (2019) 20–27.
- [2] E. Bresnahan, P. Ramadori, M. Heikenwalder, L. Zender, A. Lujambio, Novel patient-derived preclinical models of liver cancer, *J. Hepatol.* 72 (2020) 239–249.
- [3] S. Akbari, N. Arslan, S. Senturk, E. Erdal, Next-Generation liver medicine using organoid models, *Front. Cell Dev. Biol.* 7 (2019) 345.
- [4] H. Yang, L. Sun, M. Liu, Y. Mao, Patient-derived organoids: a promising model for personalized cancer treatment, *Gastroenterol. Rep. (Oxf.)* 6 (2018) 243–245.
- [5] V. Brancato, J.M. Oliveira, V.M. Correlo, R.L. Reis, S.C. Kundu, Could 3D models of cancer enhance drug screening? *Biomaterials* 232 (2020) 119744.
- [6] S. Gunti, A. Hoke, K.P. Vu, N.J. London, Organoid and spheroid tumor models: techniques and applications, *Cancers* 13 (2021).
- [7] G. Mazza, W. Al-Akkad, K. Rombouts, Engineering in vitro models of hepatofibrogenesis, *Adv. Drug Deliv. Rev.* 121 (2017) 147–157.
- [8] M. Bleijs, M. van de Wetering, H. Clevers, J. Drost, Xenograft and organoid model systems in cancer research, *EMBO J.* 38 (2019), e101654.
- [9] G.P. Risbridger, R. Toivanen, R.A. Taylor, Preclinical models of prostate cancer: patient-derived xenografts, organoids, and other Explant models, *Cold Spring Harb. Perspect. Med.* 8 (2018).
- [10] A. Collins, G.J. Miles, J. Wood, M. MacFarlane, C. Pritchard, E. Moss, Patient-derived explants, xenografts and organoids: 3-dimensional patient-relevant preclinical models in endometrial cancer, *Gynecol. Oncol.* 156 (2020) 251–259.
- [11] S. Rauth, S. Karmakar, S.K. Batra, M.P. Ponnusamy, Recent advances in organoid development and applications in disease modeling, *Biochim. Biophys. Acta Rev. Canc* 1875 (2021) 188527.
- [12] L.M. Granat, O. Kambhampati, S. Klosek, B. Niedzwecki, K. Parsa, D. Zhang, The promises and challenges of patient-derived tumor organoids in drug development and precision oncology, *Animal Model Exp. Med.* 2 (2019) 150–161.
- [13] H. Clevers, Modeling development and disease with organoids, *Cell* 165 (2016) 1586–1597.
- [14] D.F. Kaluthantrige, M. Huch, Organoids, Where we stand and where we go, *Trends Mol. Med.* 27 (2021) 416–418.
- [15] L. Sun, L. Hui, Progress in human liver organoids, *J. Mol. Cell Biol.* 12 (2020) 607–617.
- [16] P.W. Nagle, J. Plukker, C.T. Muijs, P. van Luijk, R.P. Coppes, Patient-derived tumor organoids for prediction of cancer treatment response, *Semin. Cancer Biol.* 53 (2018) 258–264.
- [17] A. Brooks, X. Liang, Y. Zhang, C.X. Zhao, M.S. Roberts, H. Wang, L. Zhang, D. Crawford, Liver organoid as a 3D in vitro model for drug validation and toxicity assessment, *Pharmacol. Res.* 169 (2021) 105608.
- [18] E.A. Castellon, Patient-derived organoids: new co-clinical model to predict treatment response in cancer? *Oral Dis* 25 (2019) 928–930.
- [19] A. Marchini, F. Gelain, Synthetic scaffolds for 3D cell cultures and organoids: applications in regenerative medicine, *Crit. Rev. Biotechnol.* (2021) 1–19.
- [20] M.A. Lancaster, M. Huch, Disease modelling in human organoids, *Dis. Model. Mech.* 12 (2019).
- [21] R. Xu, X. Zhou, S. Wang, C. Trinkle, Tumor organoid models in precision medicine and investigating cancer-stromal interactions, *Pharmacol. Ther.* 218 (2021) 107668.
- [22] K.J. Murphy, C.R. Chambers, D. Herrmann, P. Timpson, B.A. Pereira, Dynamic stromal alterations influence tumor-stroma crosstalk to promote pancreatic cancer and treatment resistance, *Cancers* 13 (2021).
- [23] Z. Gong, L. Huang, X. Tang, K. Chen, Z. Wu, L. Zhang, Y. Sun, Y. Xia, H. Chen, Y. Wei, F. Wang, S. Guo, Acoustic droplet printing tumor organoids for modeling

- bladder tumor immune microenvironment within a week, *Adv. Healthc. Mater.* 10 (2021), e2101312.
- [24] K.K. Dijkstra, C.M. Cattaneo, F. Weeber, M. Chalabi, J. van de Haar, L.F. Fanchi, M. Slagter, D.L. van der Velden, S. Kaing, S. Kelderman, N. van Rooij, M.E. van Leerdam, A. Depla, E.F. Smit, K.J. Hartemink, R. de Groot, M.C. Wolkers, N. Sachs, P. Snaebjornsson, K. Monkhorst, J. Haanen, H. Clevers, T.N. Schumacher, E. E. Voest, Generation of tumor-reactive T cells by Co-culture of peripheral blood lymphocytes and tumor organoids, *Cell* 174 (2018) 1586–1598.e12.
- [25] S. Sanegre, F. Lucantoni, R. Burgos-Panadero, L. de La Cruz-Merino, R. Noguera, N. T. Alvaro, Integrating the tumor microenvironment into cancer therapy, *Cancers* 12 (2020).
- [26] X. Yue, T.D. Nguyen, V. Zellmer, S. Zhang, P. Zorlutuna, Stromal cell-laden 3D hydrogel microwell arrays as tumor microenvironment model for studying stiffness dependent stromal cell-cancer interactions, *Biomaterials* 170 (2018) 37–48.
- [27] R. Tempest, S. Guarnerio, R. Maani, J. Cooper, N. Peake, The biological and biomechanical role of transglutaminase-2 in the tumour microenvironment, *Cancers* 13 (2021).
- [28] J. Liu, P. Li, L. Wang, M. Li, Z. Ge, L. Noordam, R. Lieshout, M. Versteeg, B. Ma, J. Su, Q. Yang, R. Zhang, G. Zhou, L.C. Carrascosa, D. Sprengers, J. IJzermans, R. Smits, J. Kwekkeboom, L. van der Laan, M.P. Peppelenbosch, Q. Pan, W. Cao, Cancer-associated fibroblasts provide a stromal niche for liver cancer organoids that confers trophic effects and therapy resistance, *Cell Mol. Gastroenterol. Hepatol.* 11 (2021) 407–431.
- [29] X. Luo, E. Fong, C. Zhu, Q. Lin, M. Xiong, A. Li, T. Li, T. Benoukraf, H. Yu, S. Liu, Hydrogel-based colorectal cancer organoid co-culture models, *Acta Biomater* 132 (2021) 461–472.
- [30] S. Kaur, I. Kaur, P. Rawal, D.M. Tripathi, A. Vasudevan, Non-matrigel scaffolds for organoid cultures, *Cancer Lett* 504 (2021) 58–66.
- [31] J.C. Mejias, M.R. Nelson, O. Liseth, K. Roy, A 96-well format microvascularized human lung-on-a-chip platform for microphysiological modeling of fibrotic diseases, *Lab Chip* 20 (2020) 3601–3611.
- [32] M. Mizuno, B. Khaledian, M. Maeda, T. Hayashi, S. Mizuno, E. Munetsuna, T. Watanabe, S. Kono, S. Okada, M. Suzuki, S. Takao, H. Minami, N. Asai, F. Sugiya, S. Takahashi, Y. Shimono, Adipin-Dependent secretion of hepatocyte growth factor regulates the adipocyte-cancer stem cell interaction, *Cancers* 13 (2021).
- [33] G. Gupta, W.H. Al-Malki, I. Kazmi, L. Thangavelu, P.K. Gupta, N.K. Jha, P. Prasher, S.K. Singh, K. Dua, The role of HGF/MET in liver cancer, *Future Med. Chem.* 13 (2021) 1829–1832.
- [34] A. Bengtsson, R. Andersson, J. Rahm, K. Ganganna, B. Andersson, D. Ansari, Organoid technology for personalized pancreatic cancer therapy, *Cell. Oncol.* 44 (2021) 251–260.
- [35] A. Nava, E. Mazza, M. Furrer, P. Villiger, W.H. Reinhart, In vivo mechanical characterization of human liver, *Med. Image Anal.* 12 (2008) 203–216.
- [36] P.O. Frappart, K. Walter, J. Gout, A.K. Beutel, M. Morawe, F. Arnold, M. Breunig, T. F. Barth, R. Marienfeld, L. Schulte, T. Ettrich, T. Hackert, M. Svinarenko, R. Rosler, S. Wiese, H. Wiese, L. Perkhofer, M. Muller, A. Lechel, B.J. Sainz, P.C. Hermann, T. Seufferlein, A. Kleger, Pancreatic cancer-derived organoids - a disease modeling tool to predict drug response, *U. Eur. Gastroenterol. J.* 8 (2020) 594–606.
- [37] T. Sato, R.G. Vries, H.J. Snippert, M. van de Wetering, N. Barker, D.E. Stange, J. H. van Es, A. Abo, P. Kujala, P.J. Peters, H. Clevers, Single Lgr5 stem cells build crypt-villus structures in vitro without a mesenchymal niche, *Nature* 459 (2009) 262–265.
- [38] S. Nuciforo, I. Fofana, M.S. Matter, T. Blumer, D. Calabrese, T. Boldanova, S. Piscuoglio, S. Wieland, F. Ringnald, G. Schwank, L.M. Terracciano, C. Ng, M. H. Heim, Organoid models of human liver cancers derived from tumor needle biopsies, *Cell Rep* 24 (2018) 1363–1376.
- [39] Q. Chen, A.Z. Chen, G. Jia, J. Li, C. Zheng, K. Chen, Molecular imaging of tumor microenvironment to assess the effects of locoregional treatment for hepatocellular carcinoma, *Hepatol. Commun.* 5 (2021), <https://doi.org/10.1002/hep4.1850>. Online ahead of print. PMID: 34738743 Review.
- [40] F. Miranda, H. Prazeres, F. Mendes, D. Martins, F. Schmitt, Resistance to endocrine therapy in HR + and/or HER2 + breast cancer: the most promising predictive biomarkers, *Mol. Biol. Rep.* 49 (1) (2021) 717–733.
- [41] O. Pos, J. Radvanszky, G. Buglyo, Z. Pos, D. Rusnakova, B. Nagy, T. Szemes, Copy number variation: characteristics, evolutionary and pathological aspects, *Biomed. J.* 44 (5) (2021) 548–559.
- [42] L. Ma, B. Diao, Z. Huang, B. Wang, J. Yu, X. Meng, The efficacy and possible mechanisms of immune checkpoint inhibitors in treating non-small cell lung cancer patients with epidermal growth factor receptor mutation, *Cancer Commun.* 41 (12) (2021) 1314–1330.
- [43] D.M. Wilson, M. Duncton, C. Chang, L.C. Lee, T.M. Georgiadis, P. Pellicena, A. M. Deacon, Y. Gao, D. Das, Early drug discovery and development of novel cancer therapeutics targeting DNA polymerase Eta (POLH), *Front. Oncol.* 11 (2021) 778925.
- [44] O.A. Deveci, E.G. Guney, S. Kaleli, E. Sahin, Immunotherapeutic role of cabazitaxel treatment in the activation of TLR3 signalling in metastatic castration-resistant prostate cancer in vitro, *Mol. Biol. Rep.* 49 (2) (2021) 1261–1271.
- [45] H. Yu, X. Zhang, W. Song, T. Pan, H. Wang, T. Ning, Q. Wei, H. Xu, B. Wu, D. Ma, Effects of 3-dimensional bioprinting alginate/gelatin hydrogel scaffold extract on proliferation and differentiation of human dental pulp stem cells, *J. Endod.* 45 (2019) 706–715.
- [46] D.J. Choi, Y. Kho, S.J. Park, Y.J. Kim, S. Chung, C.H. Kim, Effect of cross-linking on the dimensional stability and biocompatibility of a tailored 3D-bioprinted gelatin scaffold, *Int. J. Biol. Macromol.* 135 (2019) 659–667.
- [47] T. Jiang, J. Munguia-Lopez, S. Flores-Torres, J. Grant, S. Vijayakumar, A. De Leon-Rodriguez, J.M. Kinsella, Bioprintable Alginate/gelatin hydrogel 3D in vitro model systems induce cell spheroid formation, *JoVE* (137) (2018) 57826.
- [48] F. Abasalizadeh, S.V. Moghaddam, E. Alizadeh, E. Akbari, E. Kashani, S. Fazljou, M. Torbati, A. Akbarzadeh, Alginate-based hydrogels as drug delivery vehicles in cancer treatment and their applications in wound dressing and 3D bioprinting, *J. Biol. Eng.* 14 (2020) 8.
- [49] K.Y. Lee, D.J. Mooney, Alginate: properties and biomedical applications, *Prog. Polym. Sci.* 37 (2012) 106–126.
- [50] J.A. Brassard, M. Nikolaev, T. Hubscher, M. Hofer, M.P. Lutolf, Recapitulating macro-scale tissue self-organization through organoid bioprinting, *Nat. Mater.* 20 (2021) 22–29.
- [51] F. Xie, L. Sun, Y. Pang, G. Xu, B. Jin, H. Xu, X. Lu, Y. Xu, S. Du, Y. Wang, S. Feng, X. Sang, S. Zhong, X. Wang, W. Sun, H. Zhao, H. Zhang, H. Yang, P. Huang, Y. Mao, Three-dimensional bio-printing of primary human hepatocellular carcinoma for personalized medicine, *Biomaterials* 265 (2021) 120416.
- [52] M.A. Serban, A. Skardal, Hyaluronan chemistries for three-dimensional matrix applications, *Matrix Biol* 78–79 (2019) 337–345.
- [53] S.K. Kim, Y.H. Kim, S. Park, S.W. Cho, Organoid engineering with microfluidics and biomaterials for liver, lung disease, and cancer modeling, *Acta Biomater* 132 (2021) 37–51.
- [54] S.H. Au, M.D. Chamberlain, S. Mahesh, M.V. Sefton, A.R. Wheeler, Hepatic organoids for microfluidic drug screening, *Lab Chip* 14 (2014) 3290–3299.
- [55] V.S. Shirure, Y. Bi, M.B. Curtis, A. Lezia, M.M. Goedgebuure, S.P. Goedgebuure, R. Aft, R.C. Fields, S.C. George, Tumor-on-a-chip platform to investigate progression and drug sensitivity in cell lines and patient-derived organoids, *Lab Chip* 18 (2018) 3687–3702.
- [56] W. Sun, Z. Luo, J. Lee, H.J. Kim, K. Lee, P. Tebon, Y. Feng, M.R. Dokmeci, S. Sengupta, A. Khademhosseini, Organ-on-a-Chip for cancer and immune organs modeling, *Adv. Healthc. Mater.* 8 (2019), e1801363.
- [57] H. Liu, Y. Wang, K. Cui, Y. Guo, X. Zhang, J. Qin, Advances in hydrogels in organoids and organs-on-a-chip, *Adv. Mater.* 31 (2019), e1902042.
- [58] O.M. Umot, S. Ocal, C. Basdogan, G. Dogusoy, Y. Tokat, Characterization of frequency-dependent material properties of human liver and its pathologies using an impact hammer, *Med. Image Anal.* 15 (2011) 45–52.
- [59] R.G. Barr, G. Ferraioli, M.L. Palmeri, Z.D. Goodman, G. Garcia-Tsao, J. Rubin, B. Garra, R.P. Myers, S.R. Wilson, D. Rubens, D. Levine, Elastography assessment of liver fibrosis: society of radiologists in ultrasound consensus conference statement, *Radiology* 276 (2015) 845–861.
- [60] A. Guibal, C. Boullaran, M. Bruce, M. Vallin, F. Pilleul, T. Walter, J.Y. Scaozec, N. Boublay, J. Dumortier, T. Lefort, Evaluation of shearwave elastography for the characterisation of focal liver lesions on ultrasound, *Eur. Radiol.* 23 (2013) 1138–1149.
- [61] V.S. Shirure, C. Hughes, S.C. George, Engineering vascularized organoid-on-a-chip models, *Annu. Rev. Biomed. Eng.* 23 (2021) 141–167.
- [62] H. Lee, S. Chae, J.Y. Kim, W. Han, J. Kim, Y. Choi, D.W. Cho, Cell-printed 3D liver-on-a-chip possessing a liver microenvironment and biliary system, *Biofabrication* 11 (2019), 025001.
- [63] L.D. Wood, A.J. Ewald, Organoids in cancer research: a review for pathologist-scientists, *J. Pathol.* 254 (2021) 395–404.
- [64] J. Chakrabarti, V. Koh, J. So, W.P. Yong, Y. Zavros, A preclinical human-derived autologous gastric cancer organoid/immune cell Co-culture model to predict the efficacy of targeted therapies, *JoVE* (2021) 173.
- [65] M.D. Cherne, B. Sidar, T.A. Sebrell, H.S. Sanchez, K. Heaton, F.J. Kassama, M. M. Roe, A.B. Gentry, C.B. Chang, S.T. Walk, M. Jutila, J.N. Wilking, D. Bimczok, A synthetic hydrogel, VitroGel(R) ORGANOID-3, improves immune cell-epithelial interactions in a tissue chip Co-culture model of human gastric organoids and dendritic cells, *Front. Pharmacol.* 12 (2021) 707891.
- [66] I.M. Tayler, R.S. Stowers, Engineering hydrogels for personalized disease modeling and regenerative medicine, *Acta Biomater* 132 (2021) 4–22.
- [67] R.I. Aqeilan, Engineering organoids: a promising platform to understand biology and treat diseases, *Cell Death Differ* 28 (2021) 1–4.
- [68] Y.S. Zhang, A. Khademhosseini, Advances in engineering hydrogels, *Science* 356 (2017).
- [69] H. Lee, W. Han, H. Kim, D.H. Ha, J. Jang, B.S. Kim, D.W. Cho, Development of liver decellularized extracellular matrix bioink for three-dimensional cell printing-based liver tissue engineering, *Biomacromolecules* 18 (2017) 1229–1237.
- [70] C.E. Chiang, Y.Q. Fang, C.T. Ho, M. Assuncao, S.J. Lin, Y.C. Wang, A. Blocki, C. C. Huang, Bioactive decellularized extracellular matrix derived from 3D stem cell spheroids under macromolecular crowding serves as a scaffold for tissue engineering, *Adv. Healthc. Mater.* 10 (2021), e2100024.
- [71] J. Jabs, F.M. Zickgraf, J. Park, S. Wagner, X. Jiang, K. Jechow, K. Kleinheinz, U. H. Toprak, M.A. Schneider, M. Meister, S. Spaich, M. Sutterlin, M. Schlesner, A. Trumpp, M. Sprick, R. Eils, C. Conrad, Screening drug effects in patient-derived cancer cells links organoid responses to genome alterations, *Mol. Syst. Biol.* 13 (2017) 955.
- [72] D. Gao, Y. Chen, Organoid development in cancer genome discovery, *Curr. Opin. Genet. Dev.* 30 (2015) 42–48.
- [73] R. Nguyen, W.B.S. Da, L. Qiao, J. George, Developing liver organoids from induced pluripotent stem cells (iPSCs): an alternative source of organoid generation for liver cancer research, *Cancer Lett* 508 (2021) 13–17.
- [74] K.C. Lam, R.E. Araya, A. Huang, Q. Chen, M. Di Modica, R.R. Rodrigues, A. Lopes, S.B. Johnson, B. Schwarz, E. Bohrsen, A.P. Cogdill, C.M. Bosio, J.A. Wargo, M. P. Lee, R.S. Goldszmid, Microbiota triggers STING-type 1 IFN-dependent monocyte reprogramming of the tumor microenvironment, *Cell* 184 (2021) 5338–5356, e21.

- [75] L. Sun, L. Hui, Progress in human liver organoids, *J. Mol. Cell Biol.* 12 (2020) 607–617.
- [76] S. Akbari, N. Arslan, S. Senturk, E. Erdal, Next-Generation liver medicine using organoid models, *Front. Cell Dev. Biol.* 7 (2019) 345.
- [77] M. Funata, Y. Nio, D.M. Erion, W.L. Thompson, T. Takebe, The promise of human organoids in the digestive system, *Cell Death Differ* 28 (2021) 84–94.
- [78] I.M. Tayler, R.S. Stowers, Engineering hydrogels for personalized disease modeling and regenerative medicine, *Acta Biomater* 132 (2021) 4–22.
- [79] Y. Li, E. Kumacheva, Hydrogel microenvironments for cancer spheroid growth and drug screening, *Sci. Adv.* 4 (2018), eaas8998.
- [80] S. Sugimoto, E. Kobayashi, M. Fujii, Y. Ohta, K. Arai, M. Matano, K. Ishikawa, K. Miyamoto, K. Toshimitsu, S. Takahashi, K. Nanki, Y. Hakamata, T. Kanai, T. Sato, An organoid-based organ-repurposing approach to treat short bowel syndrome, *Nature* 592 (2021) 99–104.
- [81] L. Grassi, R. Alfonsi, F. Francescangeli, M. Signore, M.L. De Angelis, A. Addario, M. Costantini, E. Flex, A. Ciolfi, S. Pizzi, A. Bruselles, M. Pallocca, G. Simone, M. Haoui, M. Falchi, M. Milella, S. Sentinelli, P. Di Matteo, E. Stellacci, M. Gallucci, G. Muto, M. Tartaglia, R. De Maria, D. Bonci, Organoids as a new model for improving regenerative medicine and cancer personalized therapy in renal diseases, *Cell Death Dis* 10 (2019) 201.
- [82] A. Gough, A. Soto-Gutierrez, L. Vernetti, M.R. Ebrahimkhani, A.M. Stern, D. L. Taylor, Human biomimetic liver microphysiology systems in drug development and precision medicine, *Nat. Rev. Gastroenterol. Hepatol.* 18 (2021) 252–268.